

# The orbital evolution and gravitational waves of OJ 287 in the 4th post-Newtonian order

Balázs Kacskovics<sup>1,2,\*</sup>  and Mátyás Vasúth<sup>2</sup> 

<sup>1</sup> University of Pécs, Ifjúság út 6, 7624 Pécs, Hungary

<sup>2</sup> Wigner RCP RMKI, PO Box 49, 1525 Budapest, Hungary

E-mail: [kacskovics.balazs@wigner.hu](mailto:kacskovics.balazs@wigner.hu) and [vasuth.matyas@wigner.hu](mailto:vasuth.matyas@wigner.hu)

Received 21 September 2021, revised 28 February 2022

Accepted for publication 11 March 2022

Published 11 May 2022



CrossMark

## Abstract

We computed the orbital evolution and the emitted gravitational radiation of the supermassive black hole binary OJ 287. Here we used the initial data provided by the outburst structure of the system. We considered the spin–spin, spin–orbit, and the next-to-next leading order fourth post-Newtonian (4PN) corrections in our analysis. In this way, we could make an accurate examination of unstable orbits ( $3M < r < 6M$ ) of the secondary black hole. We tested the 4PN terms by analyzing the total and radiated energy, compared the post-Newtonian parameters and the separation of the two black holes for 3PN and 4PN. In conclusion, the 4PN corrections provided a significantly more accurate tool for analyzing unstable orbits than earlier 3PN terms. Furthermore, in this paper, we show the strain of gravitational waves emitted by OJ 287 during its complete orbital evolution including unstable orbits.

Keywords: gravitation waves, general relativity, post-Newtonism

(Some figures may appear in colour only in the online journal)

## 1. Introduction

The supermassive black hole (SMBH) binary system OJ 287 is one of the few most frequently observed astrophysical objects, which presents us with an excellent test subject for General Relativity. Owing to the fact that all of its initial parameters are given to high accuracy by [1, 2], we can analyze its entire orbital evolution. OJ 287 is located at redshift

\* Author to whom any correspondence should be addressed.



Original content from this work may be used under the terms of the [Creative Commons Attribution 4.0 licence](https://creativecommons.org/licenses/by/4.0/). Any further distribution of this work must maintain attribution to the author(s) and the title of the work, journal citation and DOI.

$z = 0.306$ , and the masses of the primary and secondary SMBHs are  $m_1 = 1.84 \times 10^{10} M_\odot$  and  $m_2 = 1.46 \times 10^8 M_\odot$  which makes the components of this system one of the most massive objects in the observable universe. For centuries, astronomers have observed and examined its quasi-periodic light variations, yet it has only recently been recognized as a blazar. The optical light curve of OJ 287 of the last  $\sim 120$  years has been showing a double periodicity of 60 years and 12 years [3, 4]. In 1996 a detailed model was introduced by Letho and Valtonen [5, 6]. In the model, the proposed 12 years orbital period is related to the major outbursts of the primary SMBH. The mechanism that forms the pair of outbursts occurring, 1 to 2 years separated, was assumed to be caused by impacts on the accretion disk of the primary SMBH by the secondary. During the transition of the secondary SMBH, matter from the accretion disk is taken away, and bremsstrahlung bursts are formed as the hot plasma becomes optically thin. This outburst structure allows us to reproduce the orbits of the binary with high accuracy. A more detailed analysis of the outburst structure can be found in [1, 2]. From the luminosity of the source, we can determine both the masses and the relative velocity. It turned out that this system has a very high velocity of  $v/c \simeq (0.06-0.26)$ , and therefore it is an ideal candidate to test strong gravitational effects.

From the timing of outbursts, Valtonen and his associates [1, 2, 7] could accurately estimate the spin of the primary SMBH and show its significance in the orbital evolution. Pihajoki [8] showed that the secondary SMBH could also produce bremsstrahlung outbursts, which implies that the secondary SMBH can also spin up. We found that in the analysis of gravitational waves (GWs), the contribution of the secondary spin is not significant enough to be considered in this article. Here we used the highest spin–spin (SS) [9, 10], spin–orbit (SO) [11, 12] terms and post-Newtonian (PN) [13–18] up to the newly released 4th PN order [19].

OJ 287 is composed of a pair of close SMBHs, and such a binary system emits intense gravitational radiation. The large amplitude of its radiation makes OJ 287 an excellent target for low-frequency gravitational-wave detectors [20]. Earlier, Zhang and his colleagues analyzed the gravitational waveform of OJ 287. They made their analysis up to 3.5PN order and their results for three periods are in harmony with the findings of Valtonen. Furthermore, they investigated the detectability of GWs emitted by the system [21]. From the frequency of the binary system, it appears that we can detect them with pulsar timing array (PTA) [22] experiments. In this paper, we extend their results by going until the start of the merger phase, with the use of fourth post-Newtonian (4PN) and spin terms. We will examine the orbital evolution and waveforms after the last stable orbit (LSO) and use OJ 287 as an experimental case for testing 4PN results.

## 2. Orbital evolution and spin effects

The inspiral of compact astrophysical objects can be described accurately in the weak-field limit, where the gravitational potential and orbital velocity are regarded as small parameters. In the PN regime [18], the motion of the binary system can be characterized as perturbed Keplerian orbits. The equation of motion and the emitted radiation of these systems are analyzed in detail by [9, 10, 15–17, 23–27]. As a result, thoroughly tested and ready to use formulas are available up to 4PN order.

To study the orbital motion, the evolution of spins and angular momenta of the binary system, we used the computational tool called CBwaves [13]. The equation of motion was integrated numerically by a fourth-order Runge–Kutta method. We determined the radiation field by a simultaneous evaluation of the analytic waveform involving all the contributions

**Table 1.** gauge conditions of radiation-reaction terms.

$\eta$	$m_1 * m_2 / (m_1 + m_2) / (m_1 + m_2)$
$\alpha$	4
$\beta$	5
$\delta_1$	$-99/14 + 27 * \eta$
$\delta_2$	$5 * (1 - 4 * \eta)$
$\delta_3$	$274/7 + 67/21 * \eta$
$\delta_4$	$5/2 * (1 - \eta)$
$\delta_5$	$-1/7 * (292 + 57 * \eta)$
$\delta_6$	$51/28 + 71/14 * \eta$

up to 2PN order. As an output of the code, both time and frequency domain waveforms are available. The PN contributions to the acceleration and the radiation field are listed in the appendices of [13].

Improving previous results on spin effects, we added 3.5PN SO contribution to the equations of motion, see e.g. [9, 14], and spin precession and the total-energy flux emitted in GWs, as it can be found in [11, 12]. Furthermore, in 2018, Blanchet *et al* [19] released the 4PN term for acceleration in the center-of-mass frame. The differential equation of the motion solved by CBwaves can be written as the sum of the following terms

$$\mathbf{a} = \mathbf{a}_{\text{PN}} + \mathbf{a}_{\text{2PN}} + \mathbf{a}_{\text{SO}} + \mathbf{a}_{\text{SS}} + \mathbf{a}_{\text{RR}} + \mathbf{a}_{\text{PN SO}} + \mathbf{a}_{\text{3PN}} + \mathbf{a}_{\text{RR1PN}} + \mathbf{a}_{\text{3.5PN SO}} + \mathbf{a}_{\text{RRSO}} + \mathbf{a}_{\text{RRSS}} + \mathbf{a}_{\text{4PN}}. \quad (1)$$

The exact form of the different contributions can be found up to 3PN in the appendix of [13]. For the sake of completeness, the newly introduced 3.5PN SO terms,  $a_{3.5\text{PN SO}}$ , spin precession, and 4PN corrections are presented here in the appendices. We used here the radiation-reaction term, derived from the Burke–Thorne radiation-reaction potential. Detailed description of the gauge parameters can be found in [17, 28] and in this paper we collected them in table 1.

We have obtained the next-to-leading order correction to the SO interaction in the center-of-mass frame up to 3.5PN order from [11], and we used is equation (3.8), which can be expressed as

$$\mathbf{a}_{3.5\text{PN SO}} = \frac{Gm}{r^3} \left[ {}^{(3.5)}\mathbf{b}_1 + {}^{(3.5)}\mathbf{b}_2 \frac{Gm}{r} + {}^{(3.5)}\mathbf{b}_3 \frac{G^2 m^2}{r^2} \right], \quad (2)$$

where the exact form of the vector coefficients ( ${}^{(3.5)}\mathbf{b}_1, {}^{(3.5)}\mathbf{b}_2, {}^{(3.5)}\mathbf{b}_3$ ) can be found in [11]. The spin evolution have been calculated in CBwaves by

$$\dot{\mathbf{S}}_1 = \frac{G}{c^2 r^3} \left\{ \Omega_1 \mathbf{L}_N - \mathbf{S}_2 - 3(\hat{\mathbf{n}} \cdot \mathbf{S}_2) \hat{\mathbf{n}} + \frac{G^2 \mu m}{c^5 r^2} \left[ \frac{2}{3} (\mathbf{v} \cdot \mathbf{S}_2) + 30 \dot{r} (\hat{\mathbf{n}} \cdot \mathbf{S}_2) \right] \mathbf{n} \right\} \times \mathbf{S}_1. \quad (3)$$

The above equation contains the standard SO and SS [16], the 2PN SO [10], the 3PN SO [11] and the 3.5PN radiative SS [26] contributions. Let us note that in CBwaves, we presume the use of covariant spin supplementary condition,  $S_A^{\mu\nu} = 0$ , where  $u_A^\mu$  is the four-velocity of the center-of-mass world line of body  $A$ , with  $A = 1, 2$ . Furthermore, we can find the spin precession correction  $\Omega_1$  to the SO contribution terms in appendix B. Here we restrict ourselves to the following form

$$\Omega_1 = \left[ \frac{1}{c^2} (\alpha_{\text{PN}} + \alpha_{\text{PN, Kidder}}) + \frac{1}{c^4} (\alpha_{2\text{PN}} + \alpha_{2\text{PN, Blanchet}}) + \frac{1}{c^6} \alpha_{3\text{PN}} + \mathcal{O} \left( \frac{1}{c^7} \right) \right]. \quad (4)$$

Simultaneously with the orbital evolution, the radiation field  $h_{ij}$  is determined by the analytic waveform contributions up to 2PN order in harmonic coordinates, valid for general eccentric and spinning sources. This can be decomposed as

$$h_{ij} = \frac{2G\mu}{c^4 D} [Q_{ij} + P^{0.5}Q_{ij} + PQ_{ij} + P^{1.5}Q_{ij} + P^2Q_{ij} + PQ_{ij}^{\text{SO}} + P^{1.5}Q_{ij}^{\text{SO}} + P^2Q_{ij}^{\text{SO}} + PQ_{ij}^{\text{SS}} + P^{1.5}Q_{ij}^{\text{tail}}], \quad (5)$$

where  $D$  is the distance to the source, and  $\mu = m_1 m_2 / (m_1 + m_2)$  is the reduced mass of the binary.  $Q_{ij}$  is the quadrupole (or Newtonian) term,  $P^{0.5}Q_{ij}$ ,  $PQ_{ij}$ ,  $P^{1.5}Q_{ij}$ ,  $P^2Q_{ij}$  [29] are higher-order relativistic corrections,  $P^{1.5}Q_{ij}^{\text{tail}}$  is the 1.5PN tail term,  $PQ_{ij}^{\text{SO}}$ ,  $P^{1.5}Q_{ij}^{\text{SO}}$ ,  $P^2Q_{ij}^{\text{SO}}$ , and  $PQ_{ij}^{\text{SS}}$  [16] are the SO and SS corrections. The full expressions of these terms are found, in detail, in the appendix of [13]. Using a fourth-order Runge–Kutta method, we could model the evolution and the emitted GWs of general binary systems with high accuracy.

Looking at a plane wave traveling in direction  $\hat{\mathbf{N}}$ , which is the unit spatial vector pointing from the center of mass of the source to the observer, the transverse-traceless (TT) part of the radiation field is provided by

$$h_{ij}^{\text{TT}} = \Lambda_{ij,kl} h_{kl}, \quad (6)$$

where

$$\Lambda_{ij,kl}(\hat{\mathbf{N}}) = \mathbf{P}_{ik}\mathbf{P}_{jl} - \frac{1}{2}\mathbf{P}_{ij}\mathbf{P}_{kl} \quad (7)$$

and

$$\mathbf{P}_{ij}(\hat{\mathbf{N}}) = \delta_{ij} - N_i N_j. \quad (8)$$

The radiation field can be defined by choosing an orthonormal triad as in [13], where

$$\hat{\mathbf{N}} = (\sin \iota \cos \phi, \sin \iota \sin \phi, \cos \iota), \quad (9)$$

$$\hat{\mathbf{p}} = (\cos \iota \cos \phi, \cos \iota \sin \phi, -\sin \iota), \quad (10)$$

$$\hat{\mathbf{q}} = (-\sin \phi, \cos \phi, 0), \quad (11)$$

and  $\iota$  and  $\phi$  are the polar angles determining the relative position of the radiation frame with respect to the source frame  $(\hat{\mathbf{x}}, \hat{\mathbf{y}}, \hat{\mathbf{z}})$ , see the first figure of [13]. The polarization states of the gravitation wave can be given, with respect to the orthonormal radiation frame, as

$$h_+ = \frac{1}{2} (\hat{p}_i \hat{p}_j - \hat{q}_i \hat{q}_j) h_{ij}^{\text{TT}}, \quad h_\times = (\hat{p}_i \hat{q}_j - \hat{q}_i \hat{p}_j) h_{ij}^{\text{TT}}. \quad (12)$$

The strain produced by the binary system at the detector can be given with the combination

$$h(t) = F_+ h_+(t) + F_\times h_\times(t), \quad (13)$$

where  $F_+$  and  $F_\times$  are the antenna pattern functions, which can be found in detailed form in [13].

**Table 2.** Initial parameters.

$m_{\odot}$	(Meter)	1476.62504
$m_1$	( $M_{\odot}$ )	$1.84 \times 10^{10}$
$m_2$	( $M_{\odot}$ )	$1.46 \times 10^8$
$r_0$	( $M$ )	$\sim 100$
$S_1/m_1^2$		0.381
$S_2/m_2^2$		0.996
$\Delta\phi$	(deg)	39.1
$e_0$		0.658

### 3. Numerical results

In our numerical analysis, we used a program package named CBwaves developed by Csizmadia *et al* [13] and maintained by our group. This package provides a fast and accurate computational tool to examine the GWs emitted by spinning eccentric binary systems. We achieve this by integrating the center-of-mass equation of motion within the PN framework up to the 4th term, plus the spin precession equations up to the 3rd term developed by Bohé *et al* [11, 12].

The initial parameters for our analysis are chosen from the estimates of Voltanen [1, 2], and Zhang *et al* [20]. The values are listed in table 2.

Where  $m_1$  is the mass of the primary SMBH and  $m_2$  is the mass of the secondary SMBH,  $r_0$  is the initial separation which we set to be approximately  $100(m_1 + m_2 = M)$ ,  $\Delta\phi$  is the precession rate of the orbit per period,  $e_0$  is the initial eccentricity of the secondary mass' orbit. We have chosen a different initial separation from the value,  $r_0 \sim 0.535 \text{ pc} \simeq 60M$ , which can be found in [20] for the sake of simplicity.

In [8], we found that both SMBH owns spin, but in our analysis, we assumed that only the primary SMBH has a spin, and it points to the positive  $\hat{z}$  direction, perpendicular to the orbital plane. In earlier computations, we have found that the contribution of the secondary SMBH's rotation is relatively small in the waveform and the orbital evolution of OJ 287. We had run simulations of the binary system in the inspiral phase and let the separation of SMBHs evolve beyond the last stable or into the so-called unstable orbit. We have estimated that the merger of the two SMBH would start slightly later than  $\sim 17\,000$  years. We stopped our simulation before the final unstable circular orbit ends, in other words, before the separation of the two bodies becomes smaller than  $r = 3M$ . With this requirement, we also prevented the event horizons from coming to contact with each other, which would be beyond the capabilities of the program package we used. The orbit of the secondary SMBH and the total and radiated energies have been presented in figure 1. As we can see, as long as the two SMBH are separated more than by  $6M$ , the total energy of the system remains seemingly constant, which means the orbit of the secondary SMBH is stable. But by looking at the radiated energy we see it almost stops growing as the orbit of the secondary SMBH converges in. It gives us some confidence that the calculations still give physically relevant results even beyond the LSO.

In order to further prove our point, we have analyzed the maximal orbital separation (apoapsis points of the elliptic orbit) and PN parameter  $\epsilon \sim (v/c)^2 \sim GM/(rc^2)$  of the 3PN- and 4PN-accurate simulations, as shown in figure 2.

As we can see in figure 2, the separation in both 3PN and 4PN approximations, marked by solid green and dashed orange lines, changes similarly. On the other hand, the PN parameters in the 3PN and 4PN approximations are different beyond the LSO. At the 3PN order equation, the PN parameter  $\epsilon \sim (v/c)^2$  has an inflection point, and it rapidly starts to decrease shortly after

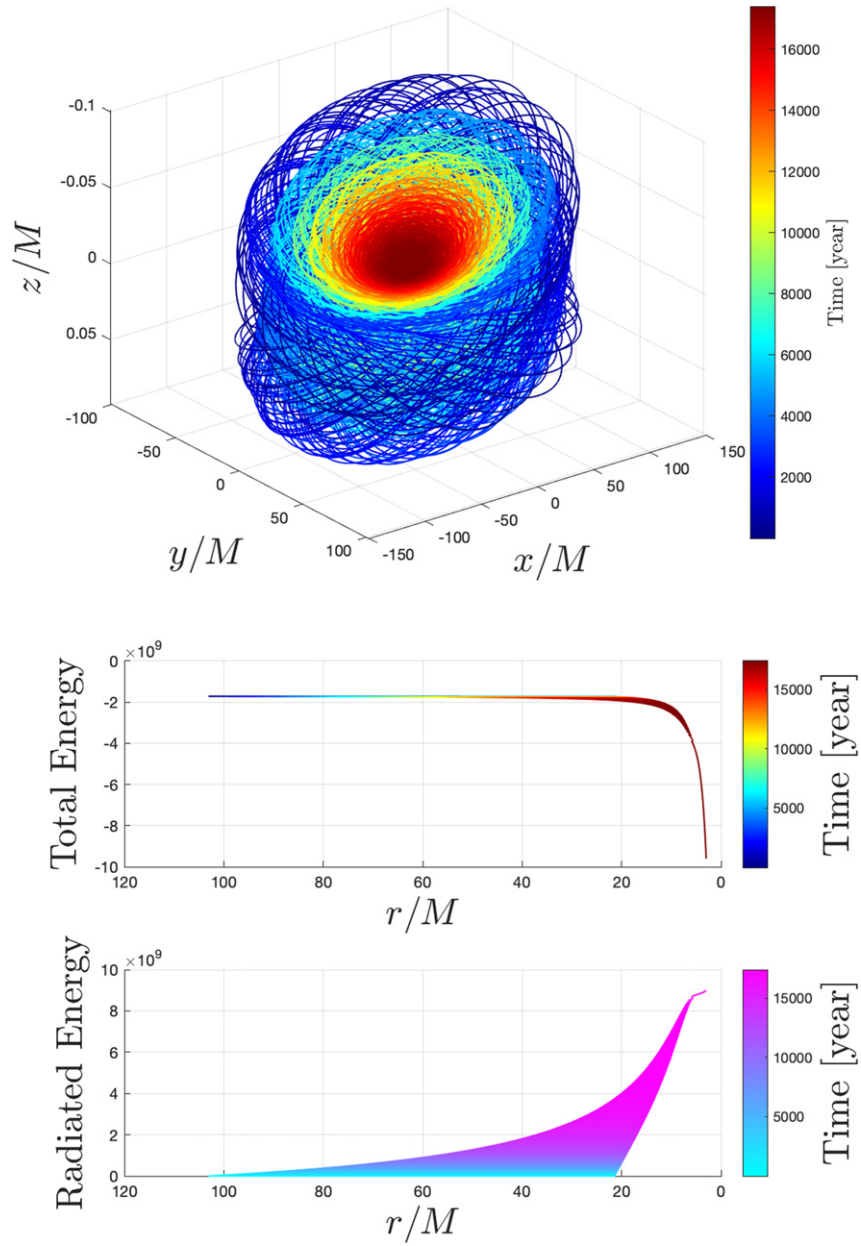


**Figure 1.** The upper panel of the figure, we can see the 4PN-accurate orbit of the secondary SMBH, whereas the central and lower panels show the total and radiated energies of the binary system in geometric units ( $E \frac{G}{c^2}$ ). Before the separation at  $3M$ , the orbit computed in our 4PN-accurate model is in good agreement with the literature and does not expose any peculiar characteristics due to numerical errors. The total and radiated energies, respectively, are in line with our prior expectations.

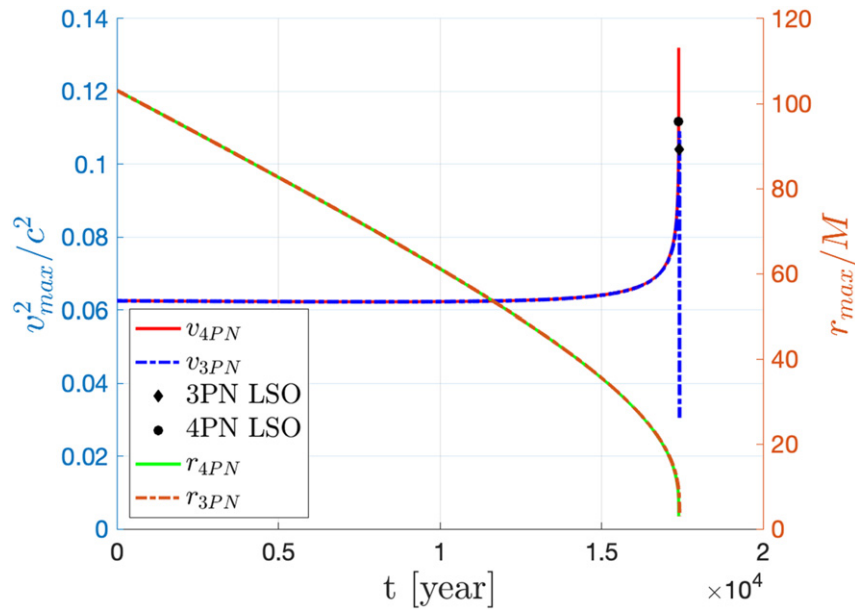


**Figure 2.** The maximal orbital separation (apoapsis points of the elliptic orbit)  $r_{\max}$  (right y axis) shows that in the early phases of the inspiral, the 4PN order's contribution is small, while we can see that the maximum speed of the center-of-mass drops in the 3PN order's chase, nearing the  $3M$  limit. We marked the beginning of the LSO with two separate markers because the secondary SMBH reaches the LSO later if we only used the corrections up to 3PN.

leaving the LSO. On the other hand, at the 4PN order equation, the PN parameter grows steadily even after the LSO. It shows that the 3PN order equation of motion changes its sign shortly after the LSO, which means the binary system starts to decouple. Consequently, the 4PN contribution provides us with a more accurate description of the orbital evolution beyond the LSO than the computations with the 3PN-accurate equation. According to reference [13], PN formalism is valid if  $\epsilon \sim 0.08$ – $0.1$ , however in section 9.6 of reference [18], Blanchet argued that the limit of the formalism is when the orbital velocities are of the order of 50% of the speed of light. In our computation, the orbital velocity was  $v = \sqrt{\epsilon} \sim 0.35c$ , in other words,  $\sim 35\%$  of the speed of light, which clearly stays well below the limit set by Blanchet.

Following the computations presented above, now we may analyze the unstable orbit in the 4PN regime. We have shown its orbital evolution in 3PN and 4PN accuracy in figure 3. The total and radiated energies of the system are shown in figure 4.

Figures 3 and 4 show further proof of our assumption, as we find more differences in the behavior orbit at 3PN and 4PN orders. We notice that the orbit at the 3PN order makes a similar number of cycles before and after the LSO. The orbit at the 4PN order reaches the  $3M$  limit within a few revolutions beyond the LSO. Furthermore, if we look at figure 4, we see that the total and radiated energies of the binary start to rapidly decrease and grow much earlier than in the 4PN term. Following the arguments presented above, we can declare that the analysis of the unstable orbit of eccentric, extreme mass ratio, supermassive binary systems require the 4PN term.

We have shown in figures 5 and 6 the strain of the GWs emitted by the binary, first for the entire orbital evolution, then for after the LSO. In order to obtain the proper amplitudes, one

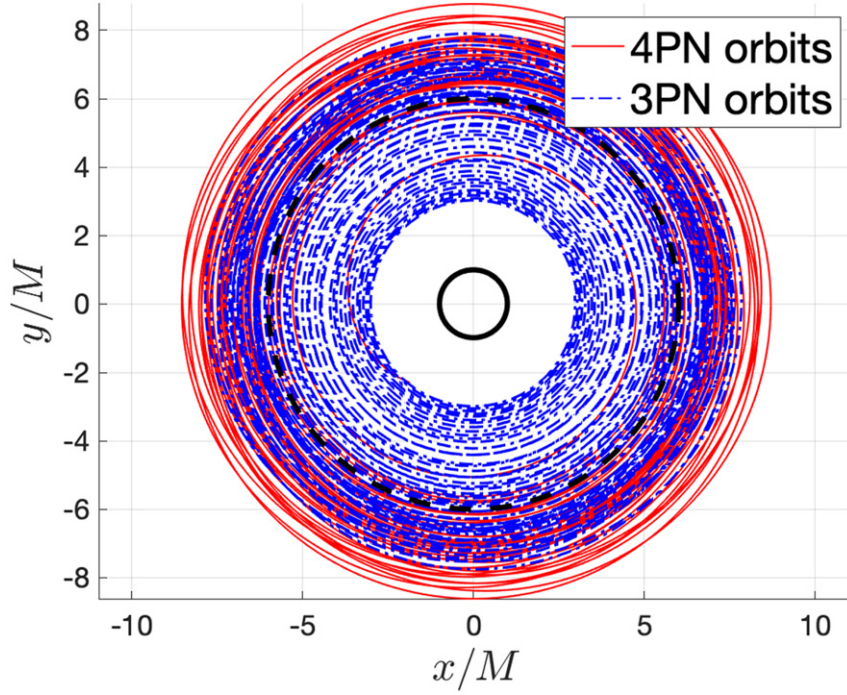


**Figure 3.** The unstable circular orbit of the secondary SMBH in 4PN and 3PN approximations are marked by the red and blue lines, respectively. For the sake of illustration, solid and dashed black circles represent the event horizon and the LSO, respectively.

has to know the distance of the source from the observer. We used the distance  $D$  found in [20] as follows

$$D_L(z) = \frac{c}{H_0} (1+z) \int_0^z \frac{dz'}{\sqrt{\Omega_m(1+z') + \Omega_\Lambda}}, \quad (14)$$

where  $\Omega_m = 0.685$ ,  $\Omega_\Lambda = 1 - \Omega_m$  are cosmological constants in a spatially flat  $\Lambda$ CDM universe, and  $H_0 = 67.3 \text{ (km s}^{-1}\text{) Mpc}^{-1}$  is the Hubble constant. Then the distance of OJ 287 is  $D = D_L(0.306) = 1.64689 \times 10^9 \text{ pc}$ , from here we can calculate the prefactor amplitude of equation (5), which is  $\frac{2G\mu}{c^4 D} = 8.6539 \times 10^{-15}$ .

As it has been demonstrated in figure 7, OJ 287 is a perfect candidate for detection techniques that target astrophysical objects like neutron stars. These methods are known as PTAs [22], and the currently ongoing experiments are the European pulsar timing array (EPTA) [30], the International pulsar timing array (IPTA) [31] and square kilometer array (SKA) [32]. Nevertheless, OJ 287's orbital frequency is insufficiently low to be detected by our current ground-based gravitational-wave interferometers. The detector sensitivity curve of these detectors and the characteristic strain of OJ 287 are presented in figure 7. The characteristic strain is attained by Fourier transformation of the GW amplitude,

$$\tilde{h} = \mathcal{F}\{h(t)\}(f) = \int_{-\infty}^{\infty} h(t) e^{-2\pi i f t} dt, \quad (15)$$

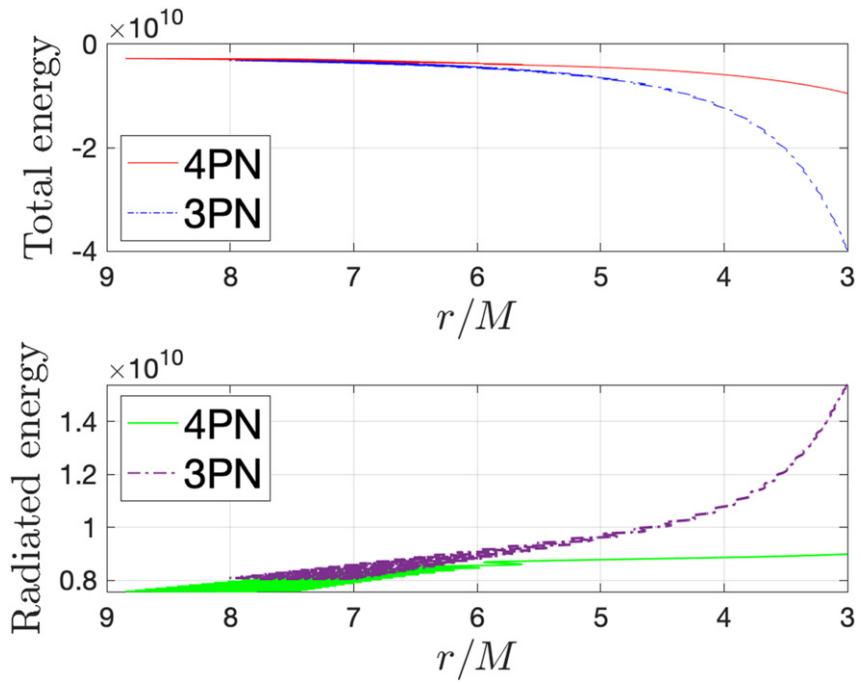


**Figure 4.** The total and the radiated energies of the unstable orbit of OJ 287 are presented in this figure. The energies are in geometric units  $\left[\frac{G}{c^4}\right]$ . This figure shows that the 4PN term makes the equation of motion numerically more accurate than stopping at the 3PN term. It means that we require the 4PN term to analyze the unstable orbit of eccentric, extreme mass ratio, supermassive binary systems.

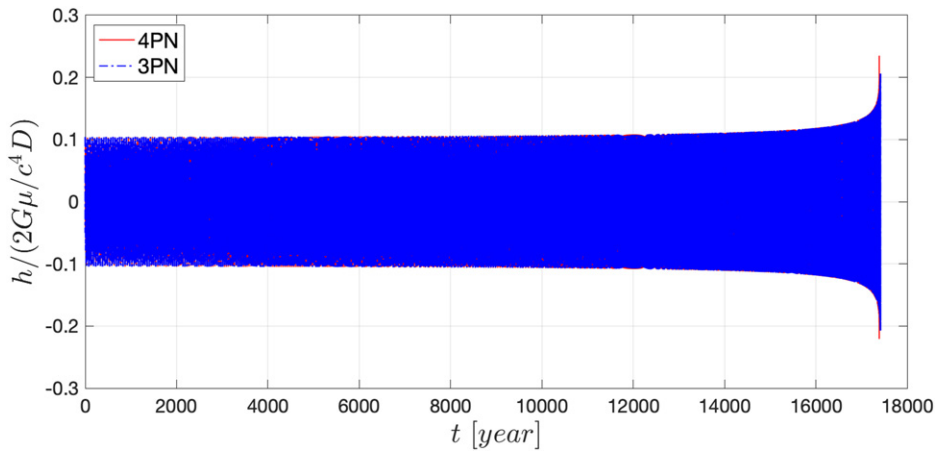


**Figure 5.** GWs emitted by the binary during its complete orbital evolution. We compared the waveforms provided by 3PN and 4PN terms.

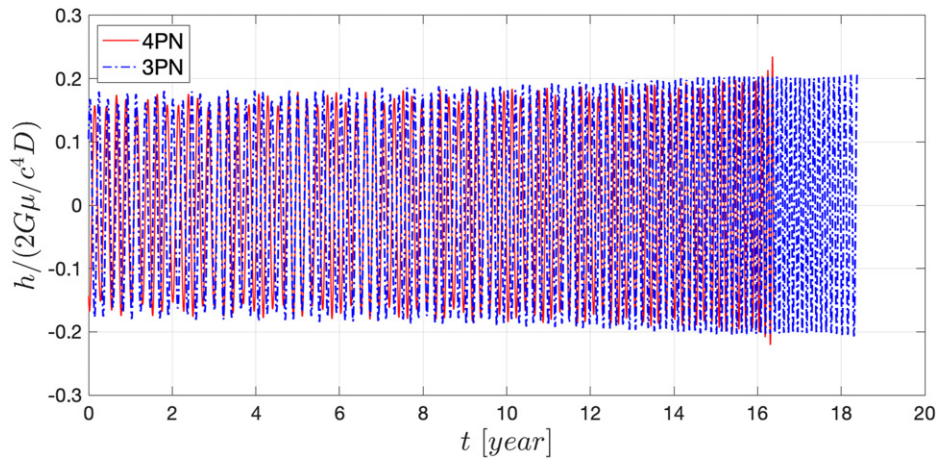


Figure 6. GWs strains emitted beyond the LSO.

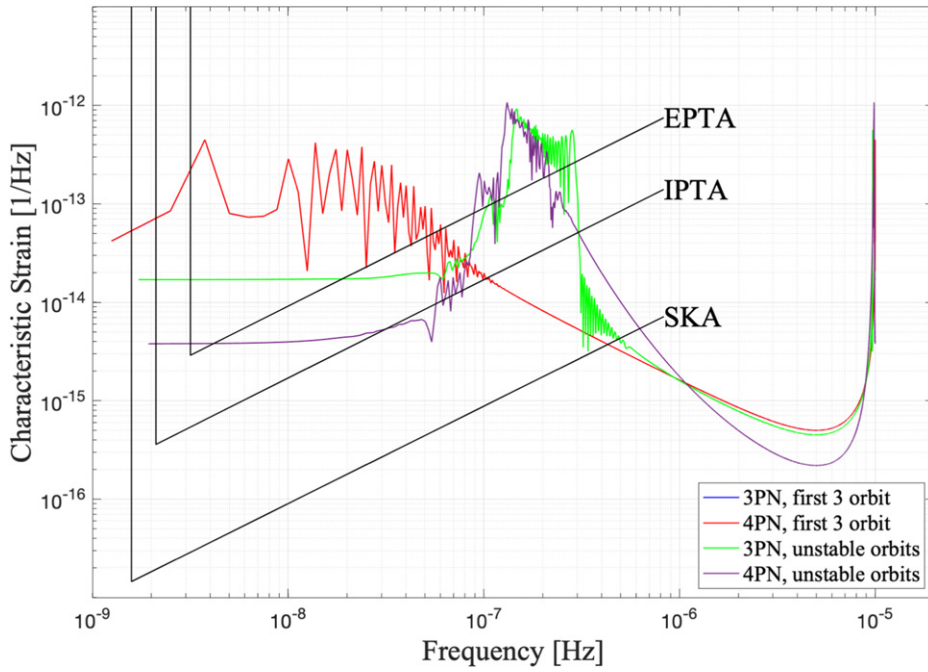


Figure 7. In this figure, we have shown the characteristic strain of OJ 287. Red and blue lines represent the strain for 4PN and 3PN initial orbit. Similarly, purple and green lines represent the strain for unstable orbit. Furthermore, we provided the detector sensitivity for EPTA, IPTA, and SKA experiments with black lines. Let us note that, for the initial orbit, the contribution of the 4PN term is so tiny that the 3PN- and 4PN-accurate strains cannot be individually distinguished by the naked eye.

as it is found in reference [33]. Then we calculated the characteristic strain for the first orbit of our simulation and the unstable orbit in 3PN and 4PN order. As we earlier have seen, the contribution of the 4PN term to the equation of motion is initially small ( $\Delta a_{3\text{PN}} \sim 10^{-32}$  and  $\Delta a_{4\text{PN}} \sim 10^{-35}$ ) compared to 3PN order.

#### 4. Conclusions

In this paper, we have studied the orbital evolution of the SMBH binary system OJ 287. We applied the PN [18] approximation up to the fourth-order correction [19] term and used the next-to-next-leading order of spin effects [9–12]. We have examined the evolution of the system beyond the LSO. By explicit computations of CBwaves, we have found that the 4PN order is essential in the evolution of orbits beyond the LSO since it makes a more numerically accurate evolution than the 3PN order. We have proved that by analyzing the total and radiated energies and the PN parameter of the system in detail, see figures 2 and 4. We have shown the waveform for the entire inspiral phase and presented the difference between the waveforms for 4PN and 3PN orders, see figure 6.

As it has been demonstrated in figure 7, OJ 287 is a perfect candidate for detection techniques that target astrophysical objects like neutron stars. These methods are known as PTAs [22] and currently, ongoing experiments are the EPTA [30], the IPTA [31] and SKA [32]. Nevertheless, OJ 287's orbital frequency is insufficiently low to be detected by our current ground-based gravitational-wave interferometers.

#### Acknowledgments

This work was supported by COST Action PHAROS (CA16214), the Hungarian NKFIH Grant Nos. 124366 and 124508. Furthermore, we would like to acknowledge the support of Wigner Scientific Computational Laboratory.

#### Data availability statement

The data that support the findings of this study are available upon reasonable request from the authors.

#### Appendix A. Center-of-mass 4th post-Newtonian order correction of the equation of mot

We can find the exact calculations of the 4th PN order in [19], therefore, for the sake of simplicity, we can write the 4th order acceleration as

$$\mathbf{a}_{4\text{PN}} = -\frac{Gm}{r^2}(\mathbf{A}\mathbf{n} + \mathbf{B}\mathbf{v}), \quad (\text{A.1})$$

where we get the  $A$  coefficient as the sum of the following terms

$$\begin{aligned}
A^{(0)} = & \left( \frac{315}{128}\eta - \frac{2205}{128}\eta^2 + \frac{2205}{64}\eta^3 - \frac{2205}{128}\eta^4 \right) i^8 + \left( -\frac{175}{16}\eta + \frac{595}{8}\eta^2 - \frac{2415}{16}\eta^3 \right. \\
& + \left. \frac{735}{8}\eta^4 \right) i^6 v^2 + \left( \frac{135}{8}\eta - \frac{1875}{16}\eta^2 + \frac{4035}{16}\eta^3 - \frac{1335}{8}\eta^4 \right) i^4 v^4 + \left( -\frac{21}{2}\eta \right. \\
& + \left. \frac{1191}{16}\eta^2 - \frac{327}{2}\eta^3 + 99\eta^4 \right) i^2 v^6 + \left( \frac{21}{8}\eta - \frac{175}{8}\eta^2 + 61\eta^3 - 54\eta^4 \right) v^8 \quad (\text{A.2})
\end{aligned}$$

$$\begin{aligned}
A^{(1)} = & \frac{m}{r} \left[ \left( \frac{2973}{40}\eta + 407\eta^2 + \frac{181}{2}\eta^3 - 86\eta^4 \right) i^6 + \left( \frac{1497}{32}\eta - \frac{1627}{2}\eta^2 \right. \right. \\
& - \left. \left. 81\eta^3 + 228\eta^4 \right) i^4 v^2 + \left( -\frac{2583}{16}\eta + \frac{1009}{2}\eta^2 + 47\eta^3 - 104\eta^4 \right) i^2 v^4 \right. \\
& + \left. \left( \frac{1067}{32}\eta - 58\eta^2 - 44\eta^3 + 58\eta^4 \right) v^6 \right] \quad (\text{A.3})
\end{aligned}$$

$$\begin{aligned}
A^{(2)} = & \frac{m^2}{r^2} \left\{ \left[ \left( \frac{2094751}{960} + \frac{45255}{1024}\pi^2 \right) \eta + \frac{326101}{96}\eta^2 - \frac{4305}{128}\eta^3 - \frac{1959}{32}\eta^4 \right] i^4 \right. \\
& + \left[ -\left( \frac{1636681}{1120} + \frac{12585}{512}\pi^2 \right) \eta - \left( \frac{255461}{112} + \frac{3075}{128}\pi^2 \right) \eta^2 - \frac{309}{4}\eta^3 \right. \\
& + \left. \left. 63\eta^4 \right] i^2 v^2 + \left[ \left( \frac{1096941}{11200} + \frac{1155}{1024}\pi^2 \right) \eta + \left( \frac{7263}{70} - \frac{123}{64}\pi^2 \right) \eta^2 \right. \right. \\
& + \left. \left. \frac{145}{2}\eta^3 - 16\eta^4 \right] v^4 \right\} \quad (\text{A.4})
\end{aligned}$$

$$\begin{aligned}
A^{(3)} = & \frac{m^3}{r^3} \left\{ \left[ -2 + \left( \frac{1297943}{8400} - \frac{2969}{16}\pi^2 \right) \eta + \left( \frac{1255151}{840} + \frac{7095}{32}\pi^2 \right) \eta^2 - 17\eta^3 \right. \right. \\
& - \left. \left. 24\eta^4 \right] i^2 \left[ \left( \frac{1237279}{252000} + \frac{3835}{96}\pi^2 \right) \eta - \left( \frac{693947}{2520} + \frac{229}{8}\pi^2 \right) \eta^2 + \frac{19}{2}\eta^3 \right] v^2 \right\} \quad (\text{A.5})
\end{aligned}$$

$$A^{(4)} = \frac{m^4}{r^4} \left[ 25 + \left( \frac{6625537}{12600} - \frac{4543}{93}\pi^2 \right) \eta + \left( \frac{477763}{420} + \frac{3}{4}\pi^2 \right) \eta^2 \right] \quad (\text{A.6})$$

and we get  $B$  coefficient similarly to  $A$  as:

$$\begin{aligned}
B^{(0)} = & \left( \frac{105}{16}\eta - \frac{245}{8}\eta^2 + \frac{385}{16}\eta^3 + \frac{35}{8}\eta^4 \right) i^7 + \left( -\frac{165}{8}\eta + \frac{1665}{16}\eta^2 \right. \\
& - \left. \frac{1725}{16}\eta^3 - \frac{105}{4}\eta^4 \right) i^5 v^2 + \left( \frac{45}{2}\eta - \frac{1869}{16}\eta^2 + 129\eta^3 + 54\eta^4 \right) i^3 v^4 \\
& + \left( -\frac{157}{16}\eta + 54\eta^2 - 69\eta^3 - 24\eta^4 \right) i v^6 \quad (\text{A.7})
\end{aligned}$$

$$B^{(1)} = \frac{m}{r} \left[ \left( -\frac{54319}{160}\eta - \frac{901}{8}\eta^2 + 60\eta^3 30\eta^4 \right) \dot{r}^5 + \left( \frac{25943}{48}\eta + \frac{1199}{12}\eta^2 \right. \right. \\ \left. \left. - \frac{349}{2}\eta^3 - 98\eta^4 \right) \dot{r}^3 v^2 + \left( -\frac{5725}{32}\eta - \frac{389}{8}\eta^2 + 118\eta^3 + 44\eta^4 \right) \dot{r} v^4 \right] \quad (\text{A.8})$$

$$B^{(2)} = \frac{m^2}{r^2} \left\{ \left[ -\left( \frac{9130111}{3360} + \frac{4695}{256}\pi^2 \right) \eta - \left( \frac{184613}{112} - \frac{1845}{64}\pi^2 \right) \eta^2 \right. \right. \\ \left. \left. + \frac{209}{2}\eta^3 + 74\eta^4 \right] \dot{r}^3 + \left[ \left( \frac{8692601}{5600} + \frac{1455}{256}\pi^2 \right) \eta \right. \right. \\ \left. \left. + \left( \frac{58557}{70} - \frac{123}{8}\pi^2 \right) \eta^2 - 70\eta^3 - 34\eta^4 \right] \dot{r} v^2 \right\} \quad (\text{A.9})$$

$$B^{(3)} = \frac{m^3}{r^3} \left[ 2 - \left( \frac{619267}{525} - \frac{791}{16}\pi^2 \right) \eta - \left( \frac{28406}{45} + \frac{2201}{32}\pi^2 \right) \eta^2 + 66\eta^3 16\eta^4 \right] \dot{r} \quad (\text{A.10})$$

where  $\eta = \mu/(m_1 + m_2)$  the reduced mass,  $\mu = m_1 m_2 / (m_1 + m_2)$ ,  $m = m_1 + m_2$  the total mass of the binary system and  $\mathbf{n} = \mathbf{r}/r$  the normal vector. Furthermore  $v^2$  is the absolute value of the speed of the center-of-mass, which we derive from  $v^2 = \mathbf{v} \cdot \mathbf{v}$ , where  $\mathbf{v} = \mathbf{v}_1 - \mathbf{v}_2$  is the relative velocity. At last  $\dot{r} = \mathbf{n} \cdot \mathbf{v}$  is the scalar product of the relative velocity and the normal vector.

Now we can turn our attention to the 4th order corrections of the  $E_{4\text{PN}} = E/\mu$  energy and  $\mathcal{L} = \mathcal{L}/\mathcal{L}_N$  orbital angular momentum of the system. First let see the terms of the energy corrections as it can be found in the 3rd section of [19]

$$\mathcal{E}^{(0)} = \left( \frac{63}{256} - \frac{1089}{256}\eta + \frac{7065}{256}\eta^2 - \frac{10143}{128}\eta^3 + \frac{21735}{256}\eta^4 \right) v^{10} \quad (\text{A.11})$$

$$\mathcal{E}^{(1)} = \frac{m}{r} \left[ \left( -\frac{35}{128}\eta + \frac{245}{128}\eta^2 - \frac{245}{64}\eta^3 + \frac{245}{128}\eta^4 \right) \dot{r}^8 + \left( \frac{25}{32}\eta - \frac{125}{16}\eta^2 + \frac{185}{8}\eta^3 \right. \right. \\ \left. \left. - \frac{595}{32}\eta^4 \right) \dot{r}^6 v^2 + \left( \frac{27}{64}\eta + \frac{243}{32}\eta^2 - \frac{1683}{32}\eta^3 + \frac{4851}{64}\eta^4 \right) \dot{r}^4 v^4 + \right. \\ \left. \times \left( -\frac{147}{32}\eta + \frac{369}{32}\eta^2 + \frac{423}{8}\eta^3 - \frac{4655}{32}\eta^4 \right) \dot{r}^2 v^6 \right. \\ \left. + \left( \frac{525}{128} - \frac{4011}{128}\eta + \frac{9507}{128}\eta^2 - \frac{357}{64}\eta^3 - \frac{15827}{128}\eta^4 \right) v^8 \right] \quad (\text{A.12})$$

$$\mathcal{E}^{(2)} = \frac{m^2}{r^2} \left[ \left( -\frac{4771}{640}\eta - \frac{461}{8}\eta^2 - \frac{17}{2}\eta^3 + \frac{15}{2}\eta^4 \right) \dot{r}^6 + \left( \frac{5347}{384}\eta + \frac{19465}{96}\eta^2 \right. \right. \\ \left. \left. - \frac{439}{8}\eta^3 - \frac{135}{2}\eta^4 \right) \dot{r}^4 v^2 + \left( \frac{15}{16} - \frac{5893}{128}\eta - \frac{12995}{64}\eta^2 + \frac{18511}{64}\eta^3 \right. \right. \\ \left. \left. + \frac{2846}{16}\eta^4 \right) \dot{r}^2 v^4 + \left( \frac{575}{32} - \frac{4489}{128}\eta + \frac{5129}{64}\eta^2 - \frac{8289}{64}\eta^3 + \frac{975}{16}\eta^4 \right) v^6 \right] \quad (\text{A.13})$$

$$\begin{aligned} \mathcal{E}^{(3)} = \frac{m^3}{r^3} & \left\{ \left[ - \left( \frac{2599\,207}{6720} - \frac{6465}{1024}\pi^2 \right) \eta - \left( \frac{103\,205}{224} - \frac{615}{128}\pi^2 \right) \eta^2 + \frac{69}{32}\eta^3 \right. \right. \\ & + \left. \frac{87}{4}\eta^4 \right] i^4 + \left[ \frac{21}{4} \left( \frac{1086\,923}{1680} + \frac{333}{512}\pi^2 \right) \eta + \left( \frac{206\,013}{560} + \frac{123}{64}\pi^2 \right) \eta^2 \right. \\ & - \left. \frac{2437}{16}\eta^3 - \frac{141}{2}\eta^4 \right] i^2 v^2 + \left[ \frac{273}{16} - \left( \frac{22\,649\,399}{100\,800} - \frac{1071}{1024}\pi^2 \right) \eta \right. \\ & \left. \left. + \left( \frac{521\,063}{10\,080} - \frac{205}{128}\pi^2 \right) \eta^2 + \frac{2373}{32}\eta^3 - \frac{45}{4}\eta^4 \right] v^4 \right\} \end{aligned} \tag{A.14}$$

$$\begin{aligned} \mathcal{E}^{(4)} = \frac{m^4}{r^4} & \left\{ \left[ \frac{9}{4} - \left( \frac{1622\,437}{12\,600} - \frac{2645}{96}\pi^2 \right) \eta - \left( \frac{289\,351}{2520} + \frac{1367}{32}\pi^2 \right) \eta^2 + \right. \right. \\ & \left. \frac{213}{8}\eta^3 + \frac{15}{2}\eta^4 \right] i^2 + \left[ \frac{15}{16} + \left( \frac{1859\,363}{16\,800} - \frac{149}{32}\pi^2 \right) \eta \right. \\ & \left. \left. + \left( \frac{22\,963}{5040} + \frac{311}{32}\pi^2 \right) \eta^2 - \frac{29}{8}\eta^3 + \frac{1}{2}\eta^4 \right] \right\} \end{aligned} \tag{A.15}$$

$$\mathcal{E}^{(5)} = \frac{m^5}{r^5} \left[ -\frac{3}{8} - \left( \frac{1697\,177}{25\,200} + \frac{105}{32}\pi^2 \right) \eta - \left( \frac{55\,111}{720} + 11\pi^2 \right) \eta^2 \right] \tag{A.16}$$

and the terms of the angular momentum, where  $\mathcal{L}_N = \mu \mathbf{r} \times \mathbf{v}$  the Newtonian term

$$\mathcal{L}^{(0)} = \left( \frac{35}{128} - \frac{605}{128}\eta + \frac{3925}{128}\eta^2 - \frac{5635}{64}\eta^3 + \frac{12\,075}{128} \right) v^8 \tag{A.17}$$

$$\begin{aligned} \mathcal{L}^{(1)} = \frac{m}{r} & \left[ \left( -\frac{5}{8}\eta + \frac{15}{8}\eta^2 + \frac{45}{16}\eta^3 - \frac{85}{16}\eta^4 \right) i^6 + \left( 3\eta - \frac{45}{4}\eta^2 - \frac{135}{16}\eta^3 \right. \right. \\ & + \left. \frac{693}{16}\eta^4 \right) i^4 v^2 + \left( -\frac{53}{8}\eta + \frac{423}{16}\eta^2 + \frac{299}{16}\eta^3 - \frac{1995}{16}\eta^4 \right) i^2 v^4 \\ & \left. + \left( \frac{75}{16} - \frac{151}{4}\eta + \frac{1553}{16}\eta^2 - \frac{425}{16}\eta^3 - \frac{2261}{16}\eta^4 \right) v^6 \right] \end{aligned} \tag{A.18}$$

$$\begin{aligned} \mathcal{L}^{(2)} = \frac{m^2}{r^2} & \left[ \left( \frac{14\,773}{320}\eta + \frac{3235}{48}\eta^2 - \frac{155}{4}\eta^3 - 27\eta^4 \right) i^4 + \left( \frac{3}{4} - \frac{5551}{60}\eta \right. \right. \\ & - \left. \frac{256}{3}\eta^2 + \frac{4459}{16}\eta^3 + \frac{569}{4}\eta^4 \right) i^2 v^2 + \left( \frac{345}{16} - \frac{65\,491}{960}\eta + \frac{12\,427}{96}\eta^2 \right. \\ & \left. \left. - \frac{3845}{32}\eta^3 + \frac{585}{8}\eta^4 \right) v^4 \right] \end{aligned} \tag{A.19}$$

$$\mathcal{L}^{(3)} = \frac{m^3}{r^3} \left\{ \left[ \frac{7}{2} + \left( \frac{7775977}{16800} + \frac{426}{256}\pi^2 \right) \eta + \frac{121449}{560}\eta^2 - \frac{1025}{8}\eta^3 - 47\eta^4 \right] i^2 + \left[ \frac{91}{4} - \left( \frac{13576009}{50400} - \frac{469}{256}\pi^2 \right) \eta + \left( \frac{276433}{5040} - \frac{41}{16}\pi^2 \right) \eta^2 + \frac{637}{8}\eta^3 - 15\eta^4 \right] v^2 \right\} \quad (\text{A.20})$$

$$\mathcal{L}^{(4)} = \frac{m^4}{r^4} \left[ \frac{15}{8} + \left( \frac{3809041}{25200} - \frac{85}{8}\pi^2 \right) \eta - \left( \frac{20131}{420} - \frac{663}{32}\pi^2 \right) \eta^2 - \frac{15}{4}\eta^3 + \eta^4 \right] \quad (\text{A.21})$$

## Appendix B. The post-Newtonian terms of the spin-orbit effects

As it is found in [10, 11, 16], we can write the 3rd PN order of the  $\Omega_1$  expression in the center of mass frame, as follows

$$\Omega_1 = \left[ \frac{1}{c^2}(\alpha_{\text{PN}} + \alpha_{\text{PN,Kidder}}) + \frac{1}{c^4}(\alpha_{2\text{PN}} + \alpha_{2\text{PN,Blanchet}}) + \frac{1}{c^6}\alpha_{3\text{PN}} + \mathcal{O}\left(\frac{1}{c^7}\right) \right]. \quad (\text{B.1})$$

where the individual corrections can be written as

$$\alpha_{\text{PN}} = \frac{Gm}{r^2} \left( \frac{3}{4} + \frac{1}{2}\eta - \frac{3}{4}\frac{\delta m}{m} \right), \quad (\text{B.2})$$

$$\alpha_{\text{PN,Kidder}} = \frac{G}{r^3} \frac{4 + 3\zeta_1}{2} \quad (\text{B.3})$$

$$\begin{aligned} \alpha_{2\text{PN}} = & \frac{Gm}{r^2} \left[ \left( -\frac{3}{2}\eta + \frac{3}{4}\eta^2 - \frac{3}{2}\eta\frac{\delta m}{m} \right) i^2 + \left( \frac{1}{16} + \frac{11}{8}\eta - \frac{3}{8}\eta^2 \right. \right. \\ & \left. \left. + \frac{\delta m}{m} \left( -\frac{1}{16} + \frac{1}{2}\eta \right) \right) v^2 \right] + \frac{G^2 m^2}{r^3} \\ & \times \left( -\frac{1}{4} - \frac{3}{8}\eta + \frac{1}{2}\eta^2 + \frac{\delta m}{m} \left( \frac{1}{4} - \frac{1}{8}\eta \right) \right), \quad (\text{B.4}) \end{aligned}$$

$$\begin{aligned} \alpha_{2\text{PN,Blanchet}} = & \frac{Gm_1^2}{8m^2 r^3} \left[ (16 + 22\zeta_1 + 10\zeta_1^2 + \zeta_1^3)v^2 - 2(4 + 7\zeta_1 + 7\zeta_1^2 \right. \\ & \left. + 2\zeta_1^3) \frac{Gm}{r} - 6(4 + 3\zeta_1)i^2 \right] \quad (\text{B.5}) \end{aligned}$$

$$\begin{aligned}
\alpha_{3\text{PN}} = & \frac{Gm}{r^2} \left[ \left( \frac{15}{8}\eta - \frac{195}{32}\eta^2 + \frac{15}{16}\eta^3 + \frac{\delta m}{m} \left( \frac{15}{8}\eta - \frac{75}{32}\eta^2 \right) \right) i^4 \right. \\
& + \left( -3\eta + \frac{291}{32}\eta^2 - \frac{45}{16}\eta^3 + \frac{\delta m}{m} \left( -3\eta + \frac{177}{32}\eta^2 \right) \right) i^2 v^2 \\
& + \left. \left( \frac{1}{32} + \frac{19}{16}\eta - \frac{31}{8}\eta^2 + \frac{17}{16}\eta^3 + \frac{\delta m}{m} \left( -\frac{1}{32} + \frac{3}{4}\eta - \frac{11}{8}\eta^2 \right) \right) v^4 \right] \\
& + \frac{G^2 m^2}{r^3} \left[ \left( \frac{1}{4} - \frac{525}{32}\eta - \frac{159}{16}\eta^2 + \frac{13}{4}\eta^3 + \frac{\delta m}{m} \left( -\frac{1}{4} - \frac{75}{32}\eta \right. \right. \right. \\
& \left. \left. - \frac{87}{16}\eta^2 \right) \right) i^2 + \left( \frac{3}{16} + \frac{27}{4}\eta + \frac{75}{32}\eta^2 - \frac{9}{8}\eta^3 \right. \\
& \left. \left. + \frac{\delta m}{m} \left( -\frac{3}{16} + \frac{9}{8}\eta + \frac{35}{32}\eta^2 \right) \right) v^2 \right] + \frac{G^3 m^3}{r^4} \\
& \times \left( \frac{7}{16} - \frac{9}{4}\eta - \frac{9}{8}\eta^2 + \frac{1}{2}\eta^3 + \frac{\delta m}{m} \left( -\frac{17}{16} - \frac{1}{8}\eta - \frac{1}{8}\eta^2 \right) \right). \tag{B.6}
\end{aligned}$$

Here  $\delta m = m_1 - m_2$  is the mass difference and  $\zeta_1 = m_1/m_2$ . We can get the expressions for  $\Omega_2$  with a simple  $\delta m \rightarrow -\delta m$  and  $\zeta_1 \rightarrow \zeta_2 = m_2/m_1$  exchange.

## ORCID iDs

Balázs Kacskovics  <https://orcid.org/0000-0001-9216-8713>

Mátyás Vasúth  <https://orcid.org/0000-0003-4573-8781>

## References

- [1] Valtonen M J *et al* 2010 Measuring black hole spin in OJ 287 *Celest. Mech. Dyn. Astron.* **106** 235–43
- [2] Valtonen M J *et al* 2010 Measuring the spin of the primary black hole in OJ 287 *Astrophys. J.* **709** 725–32
- [3] Valtonen M J *et al* 2006 Predicting the next outbursts of OJ 287 in 2006–2010 *Astrophys. J.* **646** 36–48
- [4] Valtonen M J, Gopakumar A, Mikkola S, Wiik K and Lehto H J 2014 Black hole binary OJ 287 as a testing platform for general relativity *J. Phys.: Conf. Ser.* **484** 012025
- [5] Lehto H J and Valtonen M J 1996 OJ 287 outburst structure and a binary black hole model *Astrophys. J.* **460** 207
- [6] Sundelius B, Wahde M, Lehto H J and Valtonen M J 1997 A numerical simulation of the brightness variations of OJ 287 *Astrophys. J.* **484** 180–5
- [7] Valtonen M J *et al* 2016 Primary black hole spin in OJ 287 as determined by the general relativity centenary flare *Astrophys. J. Lett.* **819** L37
- [8] Pihajoki P 2012 Outbursts from the secondary component in OJ 287 and the secondary spin-up *EPJ Web Conf.* **39** 06006
- [9] Faye G, Blanchet L and Buonanno A 2006 Higher-order spin effects in the dynamics of compact binaries: I. Equations of motion *Phys. Rev. D* **74** 104033

- [10] Blanchet L, Buonanno A and Faye G 2006 Higher-order spin effects in the dynamics of compact binaries: II. Radiation field *Phys. Rev. D* **74** 104034
- [11] Bohé A, Marsat S, Faye G and Blanchet L 2013 Next-to-next-to-leading order spin-orbit effects in the near-zone metric and precession equations of compact binaries *Classical Quantum Gravity* **30** 075017
- [12] Bohé A, Marsat S and Blanchet L 2013 Next-to-next-to-leading order spin-orbit effects in the gravitational wave flux and orbital phasing of compact binaries *Class. Quantum Grav.* **30** 135009
- [13] Csizmadia P, Debreczeni G, Rácz I and Vasúth M 2012 Gravitational waves from spinning eccentric binaries *Class. Quantum Grav.* **29** 245002
- [14] Tagoshi H, Ohashi A and Owen B J 2001 Gravitational field and equations of motion of spinning compact binaries to 2.5 post-Newtonian order *Phys. Rev. D* **63** 044006
- [15] Mora T and Will C M 2004 Post-Newtonian diagnostic of quasiequilibrium binary configurations of compact objects *Phys. Rev. D* **69** 104021
- [16] Kidder L E 1995 Coalescing binary systems of compact objects to (post)<sup>5/2</sup>-Newtonian order: V. Spin effects *Phys. Rev. D* **52** 821–47
- [17] Iyer B R and Will C M 1995 Post-Newtonian gravitational radiation reaction for two-body systems: nonspinning bodies *Phys. Rev. D* **52** 6882–93
- [18] Blanchet L 2006 Gravitational radiation from post-Newtonian sources and inspiralling compact binaries *Living Rev. Relativ.* **9** 2
- [19] Bernard L, Blanchet L, Faye G and Marchand T 2018 Center-of-mass equations of motion and conserved integrals of compact binary systems at the fourth post-Newtonian order *Phys. Rev. D* **97** 044037
- [20] Zhang Y, Wu S G and Zhao W 2013 Gravitational-wave by binary OJ 287 in 3.5 PN approximation (arXiv:1305.1122v1)
- [21] Chen J-W and Zhang Y 2018 Gravitational wave detection from OJ 287 via a pulsar timing array *Mon. Not. R. Astron. Soc.* **481** 2249–60
- [22] Hobbs G 2010 Pulsars as gravitational wave detectors (arXiv:1006.3969v1)
- [23] Damour T and Deruelle N 1981 Radiation reaction and angular momentum loss in small angle gravitational scattering *Phys. Lett. A* **87** 81–4
- [24] Gopakumar A and Iyer B R 1997 Gravitational waves from inspiraling compact binaries: angular momentum flux, evolution of the orbital elements, and the waveform to the second post-Newtonian order *Phys. Rev. D* **56** 7708–31
- [25] Will C M 2005 Post-Newtonian gravitational radiation and equations of motion via direct integration of the relaxed Einstein equations: III. Radiation reaction for binary systems with spinning bodies *Phys. Rev. D* **71** 084027
- [26] Wang H and Will C M 2007 Post-Newtonian gravitational radiation and equations of motion via direct integration of the relaxed Einstein equations: IV. Radiation reaction for binary systems with spin–spin coupling *Phys. Rev. D* **75** 064017
- [27] Arun K G, Blanchet L, Iyer B R and Qusailah M S S 2008 Inspiralling compact binaries in quasi-elliptical orbits: the complete third post-Newtonian energy flux *Phys. Rev. D* **77** 064035
- [28] Blanchet L 1993 Time-asymmetric structure of gravitational radiation *Phys. Rev. D* **47** 4392–420
- [29] Will C M and Wiseman A G 1996 Gravitational radiation from compact binary systems: gravitational waveforms and energy loss to second post-Newtonian order *Phys. Rev. D* **54** 4813–48
- [30] Kramer M and Champion D J 2013 The European pulsar timing array and the large European array for pulsars *Class. Quantum Grav.* **300** 224009
- [31] Hobbs G *et al* 2010 The international pulsar timing array project: using pulsars as a gravitational wave detector *Class. Quantum Grav.* **27** 084013
- [32] Wang Y and Mohanty S D 2017 Pulsar timing array based search for supermassive black hole binaries in the square kilometer array era *Phys. Rev. Lett.* **118** 151104
- [33] Moore C J, Cole R H and Berry C P L 2015 Gravitational-wave sensitivity curves *Class. Quantum Grav.* **32** 015014